Draft version September 14, 2016
Preprint typeset using LaTeX style emulateapj v. 5/2/11

arXiv:1609.03586v1 [astro-ph.SR] 12 Sep 2016

LONG-TERM, MULTIWAVELENGTH LIGHT CURVES OF ULTRA-COOL DWARFS: I. AN INTERPLAY OF STARSPOTS & CLOUDS LIKELY DRIVE THE VARIABILITY OF THE L3.5 DWARF 2MASS 0036+18

Bryce Croll[1], Philip S. Muirhead[1 2], Eunkyu Han[2], Paul A. Dalba[2], Jacqueline Radigan[3], Caroline V. Morley[4], Marko Lazarevic[5], Brian Taylor[6]

Draft version September 14, 2016

ABSTRACT

We present multi-telescope, ground-based, multiwavelength optical and near-infrared photometry of the variable L3.5 ultra-cool dwarf 2MASSW J0036159+182110. We present 22 nights of photometry of 2MASSW J0036159+182110, including 7 nights of simultaneous, multiwavelength photometry, spread over ∼120 days allowing us to determine the rotation period of this ultra-cool dwarf to be 3.080 ± 0.001 hr. Our many nights of multiwavelength photometry allow us to observe the evolution, or more specifically the lack thereof, of the light curve over a great many rotation periods. The lack of discernible phase shifts in our multiwavelength photometry, and that the amplitude of variability generally decreases as one moves to longer wavelengths for 2MASSW J0036159+182110, is generally consistent with starspots driving the variability on this ultra-cool dwarf, with starspots that are ∼100 degrees K hotter or cooler than the ∼1700 K photosphere. Also, reasonably thick clouds are required to fit the spectra of 2MASSW J0036159+182110, suggesting there likely exists some complex interplay between the starspots driving the variability of this ultra-cool dwarf and the clouds that appear to envelope this ultra-cool dwarf.

Subject headings: brown dwarfs – techniques: photometric – stars: rotation – stars: individual: 2MASSW J0036159+182110

1. INTRODUCTION

Detecting and characterizing the variability of ultra-cool dwarfs is an area that has attracted growing attention in recent years, with a wealth of variability detections from the late-M, L & T spectral classes (e.g. Gelino et al. 2002; Irwin et al. 2011; Radigan et al. 2014; Buenzli et al. 2014; Metchev et al. 2015). For L-dwarfs, ground and space-based optical, near-infrared and infrared observations have recently shown that low level variability of L-dwarfs is common (Bailer-Jones & Mundt 2001; Gelino et al. 2002; Lane et al. 2007; Harding et al. 2013; Koen 2013; Metchev et al. 2015); intriguingly, once viewing geometry is taken into account, all L-dwarfs might be variable (Metchev et al. 2015). The questions this prompts are: what is the astrophysical cause of the observed variability, is it consistent across the L-spectral class, and if not where does the transition region lie between various astrophysical causes of the observed variability.

On the stellar side of the hydrogen-fusing limit, starspots are the usual explanation for the observed variability. M-dwarfs are notoriously active, with detections of Hα, a common marker of activity, rising throughout the M-spectral class, including that nearly all very late M-dwarfs are active (West et al. 2004; Schmidt 2015). Rotation periods revealed by photometry (Rockenfeller et al. 2006; Irwin et al. 2011), and Doppler imaging techniques for M-dwarfs (Barnes & Collier Cameron 2001; Barnes et al. 2004), have indicated that starspots are ubiquitous on M-dwarfs.

Until recently there was reason to doubt that this starspot driven variability extended into the L-spectral class. The neutral atmospheres of L dwarfs were believed to be too electrically resistive, with too small of magnetic Reynolds numbers, for magnetic starspots to form (Mohanty et al. 2002; Gelino et al. 2002). This conclusion was previously supported by studies that found the frequency of Hα detections fell sharply at the M/L transition, reaching negligible levels by the ∼L3 spectral class (West et al. 2004). This did not stop speculation that the variability displayed by L-dwarfs might arise from magnetic starspots (Clarke et al. 2002; Lane et al. 2007). Such speculation might prove to be prescient, as a recent study has cast doubts on previous Hα null-detections for L-dwarfs and therefore indicated that starspots might be present throughout the L spectral class: Schmidt (2015) analyzed higher signal-to-noise L-dwarf spectra and were able to detect Hα for approximately 90% of L0 dwarfs, and more than half of L-dwarfs as late as L5. Therefore, starspots might be driving the variability for cloudy early and even-late L dwarfs.

Once ultra-cool dwarf effective temperatures drop and silicate clouds begin to clear at the L/T transition, cloud condensate variability has become the accepted explanation for the large amplitude variability that has been observed for these objects (Artigau et al. 2009; Radigan et al. 2012; Gillon et al. 2013; Radigan et al. 2014; Buenzli et al. 2014; Crossfield et al. 2014b). Multiwavelength photometry of these apparent cloudy ultra-cool dwarfs has returned light curves with differ-

[1] Institute for Astrophysical Research, Boston University, 725 Commonwealth Ave. Room 506, Boston, MA 02215; croll@bu.edu
[2] Department of Astronomy, Boston University, 725 Commonwealth Ave., Boston, MA 02215, USA
[3] Utah Valley University, Orem, UT 84058, USA
[4] Department of Astronomy and Astrophysics, University of California, Santa Cruz, CA 95064, USA
[5] Department of Physics, Northeastern University, 100 Forsyth St, Boston, MA 02115
[6] TI Research, 2915 Kletha Trail, Flagstaff Az. 86005

ent amplitudes at different wavelengths (Radigan et al. 2012), and with significant temporal phase shifts in the observed variability at different wavelengths (Buenzli et al. 2012; Yang et al. 2016), including multi-wavelength light curves that are anti-correlated in phase (Biller et al. 2013). However, multiwavelength light curves of some of these brown dwarfs that display variability that is believed to be driven by heterogeneous cloud cover have not displayed significant phase offsets (Apai et al. 2013; Buenzli et al. 2015). The likely explanation is that multiwavelength phase shifts will not be caused by cloud variability if the clouds span multiple pressure layers, and specifically, if the clouds span the range of pressures that are probed by the various wavelengths of observation.

Intriguingly, cloud condensate variability might not be constrained to the L/T transition. Spitzer/IRAC observations have indicated that nearly all L-dwarfs are likely variable (Metchev et al. 2015), and anti-correlated light curves have been observed on a late-M dwarf (Littlefair et al. 2008) – in both cases clouds are a likely explanation for the observed variability.

Another possibility that has recently arose, is that the observed variability of ultra-cool dwarfs results from auroral activity, similar to the aurorae observed on planets in our own solar system (e.g. Clarke et al. 1980) including the Earth. Such auroral activity has been observed at the end of the main sequence on an M8.5 dwarf (Hallinan et al. 2015). Multiwavelength photometry of this dwarf displays light curves that are anti-correlated in phase, and Hallinan et al. (2015) speculate that auroral activity might explain the anti-correlated light curves of another late M-dwarf (Littlefair et al. 2008). Similar auroral activity may be indicated from radio detections of polarized, pulsed emissions from a T2.5 dwarf (Kao et al. 2016) and a T6.5 dwarf (Route & Wolszczan 2012; Williams & Berger 2015). Therefore, another possibility is that auroral activity may be responsible for some of the variability at the L/T transition (Artigau et al. 2009; Radigan et al. 2012) that has previously been believed to be due to holes in condensate clouds.

Finally, another explanation for the observed variability is atmospheric temperature variations, arising either deep in the atmosphere of these ultra-cool dwarfs, or at other pressure layers, that are communicated via radiative heating to the altitude regions that are probed by optical to near- and mid-infrared observations (Showman & Kaspi 2013; Robinson & Marley 2014; Morley et al. 2014).

It is also possible that ultra-cool dwarfs are variable due to more than one of the aforementioned astrophysical reasons. Time evolving clouds may periodically obscure magnetically driven cool or hot starspots (Lane et al. 2007; Heinze et al. 2013; Metchev et al. 2015), or aurorae may play an occasional role on predominantly cloudy brown dwarfs (Hallinan et al. 2015). Many variability studies of ultra-cool dwarfs to date have examined targets for only tens of minutes (Buenzli et al. 2014) to hours at a time (Radigan et al. 2014). This method is likely sufficient for ultra-cool dwarfs that display constant variability (Gizis et al. 2013, 2015), but will inadequately address the variability of objects with light curves that evolve rapidly, such as have been observed for several ultra-cool dwarfs (Artigau et al. 2009; Gillon et al. 2013; Metchev et al. 2015). The rapid evolution of these brown dwarfs might be due to the properties of a single variability mechanism changing — such as the size of starspots growing, or the thickness of clouds decreasing — but could also be due to the growing or waning strength of a secondary variability mechanism compared to the primary mechanism. It is therefore imperative to monitor ultra-cool dwarfs for multiple rotation cycles spread over days, weeks, months and even years.

Precise long-term monitoring of ultra-cool dwarfs is also a perfect data-set to search for transiting exoplanets that are as small or smaller than Earth-sized planets in the "habitable zones" of these dwarfs. Ultra-cool dwarfs typically have stellar radii similar to that of Jupiter (Charbrier et al. 2000), meaning that even Earth-sized planets produce ∼1% transit depths. For late M to early T dwarf spectral types the habitable zones stretch from periods of a day, up to a few days (depending on the influence of various atmospheric compositions and albedos, and the exact effects of tidal heating; Bolmont et al. 2011; Barnes & Heller 2013; Zsom et al. 2013). The number of small planets appears to increase with decreasing stellar effective temperature (Howard et al. 2012; Dressing & Charbonneau 2015) – trends that may continue into the substellar regime. There are already examples of M-dwarfs orbited by multiple rocky planets in short orbits: there are three rocky planets with periods less than two days orbiting an M4 dwarf (Muirhead et al. 2012), and two rocky planets have been found to orbit an M8 dwarf with an additional rocky planet in a longer period orbit (Gillon et al. 2016). Perhaps most importantly, a habitable rocky planet around an ultra-cool dwarf would be more favourable for follow-up than hosts with earlier spectral types; atmospheric spectral features of a planet around a brown dwarf should prove detectable with a feasible two weeks of total *James Webb Space Telescope* observing time (Belu et al. 2013).

Here we attempt to characterize and determine the astrophysical cause of the variability for 2MASSW J0036159+182110; in Section 2 we provide an overview of this intriguing L3.5 ultra-cool dwarf. To determine the physical mechanism causing the variability of 2MASSW J0036159+182110 in Section 3 we present 22 nights of photometry of 2MASSW J0036159+182110 spread out over ∼120 days, from optical to near-infrared wavelengths (the Ks, H, J, I, z' and R-bands), including 7 nights of simultaneous multiwavelength photometry in the optical and the near-infrared. In Section 4 we analyze our multiwavelength photometry and determine that the rotation period of this ultra-cool dwarf is approximately 3.080 ± 0.001 hr, and this is consistent from wavelength to wavelength for our optical and near-infrared photometry and the previously detected radio period, allowing us to place a limit on differential rotation for 2MASSW J0036159+182110. We also demonstrate a lack of significant phase offsets in our simultaneous multiwavelength variability, and therefore starspots rotating in and out of view, or gaps in clouds that span multiple pressure layers probed by our observations, are the most likely explanations for the observed variability on 2MASSW J0036159+182110. Our photometry does not reveal any significant flares, such as have been observed at radio wavelengths, and we are therefore able to place a limit on

the frequency of flaring for this ultra-cool dwarf (Section 5). We also rule out the presence of transiting super-Earth sized planets in the habitable zone of this ultra-cool dwarf (Section 6). In Section 7 we demonstrate that the decreasing amplitudes of variability that we observe with increasing wavelength in our photometry are most consistent with starspots or gaps in clouds that are that are approximately $\sim$100 K cooler or hotter than the photosphere of this ultra-cool dwarf. In Section 8 we conclude that the variability we observe from 2MASS 0036+18 is likely driven by starspots, but there probably exists some complex interplay between starspots and the clouds that appear to envelope this ultra-cool dwarf.

2. THE L3.5 ULTRA-COOL DWARF 2MASS 0036+18

The L3.5 ultra-cool dwarf 2MASSW J0036159+182110 (hereafter 2MASS 0036+18) has been subject to intensive multiwavelength photometric observations: from the X-ray and radio (Berger 2002; Berger et al. 2005), to the optical and near-infrared (Gelino et al. 2002; Lane et al. 2007; Maiti et al. 2007; Koen 2013; Harding et al. 2013), and also the infrared (Metchev et al. 2015). At several of these wavelengths 2MASS 0036+18 has been reported to be variable. Berger et al. (2005) detected periodic radio emission from 2MASS 0036+18 with a period of $\sim$3 hr, but failed to detect X-ray or Hα emission from this dwarf. Hallinan et al. (2008) observed 2MASS 0036+18 in the radio for 12 hours and observed a periodicity of 3.08 $\pm$ 0.05 hours that was attributed to rotation & the electron cyclotron maser instability. 2MASS 0036+18 was announced as an L-dwarf by Kirkpatrick et al. (2000), and is believed to be at or below the hydrogen burning limit (Hallinan et al. 2008). Vrba et al. (2004) inferred an effective temperature of $\sim$1900 K, although a model fit to spectra of this ultra-cool dwarf suggest a slightly lower effective temperature of $\sim$1700 K (Cushing et al. 2008).

Optical and very near-infrared photometric monitoring has led to a confusing mixture of detections and upper-limits on variability, possibly due to the impact of systematic errors in the optical and near-infrared: (i) Gelino et al. (2002) found 2MASS 0036+18 to not be obviously variable in the I-band above their precision of $\sim$1%, (ii) Maiti et al. (2007) reported that 2MASS 0036+18 was likely variable in several nights of quasi-simultaneous R and I-band observations, and variable in R-band but not in I-band on one night; inspection of the Maiti et al. (2007) light curves indicate that statistical and systematic errors in their photometry limit the wider applicability of their conclusions, (iii) Lane et al. (2007) reported up to 5% peak-to-peak I-band variability of 2MASS 0036+18 from a single night of photometric monitoring, (iv) Koen (2013) reported 2MASS 0036+18 to be variable in I-band on two nights, and not variable in R-band on the second night that was contemporaneous with their I-band variability detection, (v) Harding et al. (2013) found 2MASS 0036+18 to be variable at the 4% level from two nights of I-band photometry, although these data were affected by heavy clouds. Most recently, Metchev et al. (2015) used Spitzer/IRAC (Fazio et al. 2004) to obtain 8 hours of 3.6 μm photometry immediately followed by 6 hours of 4.5 μm photometry of 2MASS 0036+18; the ultra-cool dwarf displayed variability with a period of $\sim$2.7 h that appeared to evolve from rotation period to rotation period with peak-to-peak amplitudes of 0.47 $\pm$ 0.05% at 3.6 μm and 0.19 $\pm$ 0.04% at 4.5 μm. Although, the smaller amplitude variability displayed in the 4.5 μm channel than the 3.6 μm channel is consistent with what one expects if the variability is due to cool starspots on 2MASS 0036+18, as the two channel photometry is not simultaneous, and this ultra-cool dwarf appears to display irregular variability that rapidly evolves, this conclusion is not definitive.

Furthermore, after a number of searches for Hα that resulted in null-results (Kirkpatrick et al. 2000; Berger et al. 2005; Reiners & Basri 2008), recently Pineda et al. (2016) detected Hα emission from 2MASS 0036+18, suggesting the possibility of intermittent Hα emission from this ultra-cool dwarf.

Therefore the detections of variability of 2MASS 0036+18 to date may be the result of a single physical process, or the result of more than one physical process occuring simultaneously or at different epochs in time. The likely physical mechanisms leading to the observed variability include: starspots, aurorae, cloud variability, temperature fluctuations, etc. The radio period, apparent intermittent Hα emission, and various optical and near-infrared variability detections to date, suggest that 2MASS 0036+18 is active and starspots are a likely physical mechanism driving the variability of this ultra-cool dwarf. Here we present considerable additional ground-based observations of 2MASS 0036+18 to determine whether starspots, or another physical mechanism, is driving the observed variability of this ultra-cool dwarf.

3. OBSERVATIONS

We observed the ultra-cool dwarf 2MASS 0036+18 on 22 nights spread out over $\sim$120 days. Observations were conducted using the Perkins 1.8-m telescope, the Hall 1.1-m telescope, and the 4.3-m Discovery Channel Telescope (DCT). On the Perkins telescope our photometry was obtained using either the PRISM (Janes et al. 2004) instrument in the optical and very near-infrared, or the Mimir instrument (Clemens et al. 2007) in the near-infrared. On the Hall telescope we used the NASA42 imager, and on the DCT we used the Large Monolithic Imager (LMI; Massey et al. 2013). We summarize our observations in Table 1.

Whenever possible we attempted to observe the same target with two different telescopes at the same time at different wavelengths. For our 2015 October 14 (UTC) observations of 2MASS 0036+18 we achieved multiwavelength observations of this target by switching the DCT filter wheel back and forth between the z' and R-band filters. Six 60-second exposures were conducted in R-band, followed by thirteen 20-second in z'-band and then the process was repeated. In addition to the $\sim$8.5 s overhead for reading out the chip, there was an additional overhead for switching the filter wheel that was usually $\sim$30 s. For our DCT/LMI observations we utilized 4-amplifier read-out and 2x2 pixel binning to improve the duty-cycle.

Our red-optical and very near-infrared data using the Hall/NASA42 CCD feature significant fringing, due to thin-film interference patterns from the thin CCD and atmospheric emission lines. To eliminate this obvious fringing we produced night-time fringe frames using the

TABLE 1
Observing Log

Date (UTC)	Telescope & Instrument	Band	Duration[a] (hours)	Exposure Time (sec)	Overhead[b] (sec)	Airmass	Conditions	Aperture [c] (pixels)
2015/08/20	Perkins/MIMIR	J	6.32	15	3	2.04 → 1.04 → 1.15	Clear	5.5, 15, 25
2015/08/22	Perkins/MIMIR	J	4.05	15	3	1.20 → 1.04 → 1.15	Clear	6, 15, 25
2015/08/23	Perkins/MIMIR	J	4.63	15	3	1.36 → 1.04 → 1.13	Clear	6, 15, 25
2015/08/29	Perkins/MIMIR	J	2.94	15	3	1.04 → 1.33	Thin clouds at the start	6, 15, 25
2015/08/30	Perkins/MIMIR	J	6.93	10, 15	3	1.66 → 1.04 → 1.41	Occasional clouds	5, 15, 25
2015/09/01	Perkins/MIMIR	J	6.08	15, 20	3	1.80 → 1.04 → 1.10	Occasional thick clouds	5, 15, 25
2015/09/02	Perkins/MIMIR	J	4.61	15, 20	3	1.12 → 1.04 → 1.38	Occasional clouds	6, 15, 25
2015/09/03	Perkins/MIMIR	J	5.68	20	3	1.24 → 1.04 → 1.45	Occasional clouds	5, 15, 25
2015/09/23	Perkins/PRISM	I	5.91	20	18	1.12 → 1.04 → 1.99	Clear	7, 15, 27
2015/09/23	Hall/NASA42	I	4.71	180	9	1.05 → 1.04 → 2.06	Clear	4.5, 14, 26
2015/09/24	Perkins/PRISM	z'	5.38	40	18	1.11 → 1.04 → 1.68	Clear	7, 15, 27
2015/09/24	Hall/NASA42	I	5.78	180	9	1.09 → 1.04 → 2.10	Clear	4.5, 14, 26
2015/09/25	Perkins/PRISM	R	8.91	150	18	1.89 → 1.04 → 2.27	Clear	6, 15, 27
2015/09/25	Hall/NASA42	z'	8.64	100	9	1.67 → 1.04 → 2.38	Clear	4.5, 14, 26
2015/09/26	Perkins/PRISM	R	9.01	150	18	1.95 → 1.04 → 2.27	Clear	6, 15, 27
2015/09/26[d]	Hall/NASA42	z'	8.56	100	9	1.64 → 1.04 → 2.38	Clear	4.5, 14, 26
2015/09/29	Perkins/PRISM	z'	9.41	50	18	2.25 → 1.04 → 2.30	Thin clouds	7, 15, 27
2015/10/14	DCT/LMI	z' & R	8.49	20, 60	8.5	1.63 → 1.04 → 2.31	Clear	8, 20, 30
2015/11/07	Perkins/MIMIR	J	3.52	20	3	1.06 → 1.90	Clear	5, 15, 25
2015/11/08	Perkins/MIMIR	J	7.97	15, 20	3	1.46 → 1.04 → 2.26	Clear	7, 15, 25
2015/11/08	Hall/NASA42	I	7.09	180	9	1.29 → 1.04 → 2.03	Clear	4.5, 14, 26
2015/11/09	Perkins/MIMIR	H	7.73	5,6,7	3	1.40 → 1.04 → 2.20	Clear	5.5, 15, 25
2015/11/09	Hall/NASA42	I	8.23	180	9	1.55 → 1.04 → 2.26	Clear	4.5, 14, 26
2015/11/11	Perkins/MIMIR	Ks	4.31	20	3	1.16 → 1.04 → 1.24	Clear	10, 15, 25
2015/11/23	Perkins/MIMIR	J	7.50	10	3	1.37 → 1.04 → 2.09	Clear	4.5, 15, 25
2015/11/24	Perkins/MIMIR	J	7.71	10	3	1.36 → 1.04 → 2.33	Clear	6, 15, 25
2015/11/26	Perkins/MIMIR	J	2.75	20	3	1.05 → 1.04 → 1.21	Steady thin clouds	6, 15, 25
2015/12/16	Hall/NASA42	z'	4.96	180	9	1.09 → 1.04 → 1.64	Clear	4.5, 14, 26
2015/12/18	Perkins/MIMIR	J	6.50	15	3	1.09 → 1.04 → 2.96	Clear	6, 15, 25

[a] The duration indicates the time between the first and last observation of the evening, and does not take into account gaps in the data due to clouds, humidity or poor weather.
[b] The overhead includes time for read-out, and any other applicable overheads.
[c] We give the radius of the aperture, the radius of the inner annulus and the radius of the outer annulus that we use for sky subtraction in pixels.
[d] For this data fringes were removed using the technique discussed in Section 3.

same band of observation and subtract the fringes from each individual frame using the technique detailed by Snodgrass & Carry (2013). We noticed that this technique only improved the photometry in a handful of cases when there was significant movement of the point-spread-function of the target and reference stars due to poor telescope tracking. We therefore only apply this technique to a few Hall/NASA42 data-sets that we denote in Table 1.

The DCT/LMI, Hall/NASA42, and Perkins/PRISM data are processed by bias subtracting the data, while the Perkins/Mimir data are dark-subtracted. For our DCT/LMI & Hall/NASA42 we use a twilight flat to sky-flat the data, while for our Perkins/Mimir data we use a dome flat.

We do not perform a non-linearity correction on our Perkins/Mimir data. We attempted to utilize the non-linearity correction employed by Clemens et al. (2007), but noticed this method simply added noise to our Perkins/Mimir photometric data-sets. The peak pixel value in our target and reference stars for our Perkins/Mimir photometry is often displayed by 2MASS J00360421+1819309, a star we frequently use as a reference star. Although the peak pixel value of 2MASS J00360421+1819309 often reaches ADU values (∼8000) where non-linearity correction is likely important (Clemens et al. 2007), the vast majority of pixels we utilize in our apertures are at much more modest illumination values. Also as we employ differential photometry the impact of an incorrect non-linearity correction is mitigated; for instance, our SIMP J013656.5+093347 & TVLM 513-46546 Perkins/Mimir photometry (Croll et al. 2016) displays very similar light curves utilizing the Clemens et al. (2007) non-linearity correction or no non-linearity correction whatsoever.

Aperture photometry is then performed on all Perkins, Hall and DCT data-sets using the techniques discussed in Croll et al. (2015) and references therein. The size of the aperture radii, and the inner and outer radii of the annuli we use for sky subtraction are indicated in Table 1. Due to the obvious variability of 2MASS 0036+18, it is difficult to determine the uncertainties on our differential photometry from the photometry of 2MASS 0036+18 alone; instead the uncertainties for each observing session are assigned from the RMS of the photometry of reference stars that are similarly bright as the target. This technique is employed and described in detail for Croll et al. (2015b).

We plot our multiwavelength DCT, Perkins & Hall data in Figure 1 & 2.

4. THE VARIABILITY OF 2MASS 0036+18

4.1. *The Rotation Period of 2MASS 0036+18*

We present Lomb-Scargle periodograms (Lomb 1976; Scargle 1982) of all our data in Figure 3. The variable, near-sinusoidal light curves often displayed by 2MASS 0036+18 are well-suited to period finding utilizing a Lomb-Scargle periodogram. The apparent rotation period from the Lomb-Scargle periodogram of all our data

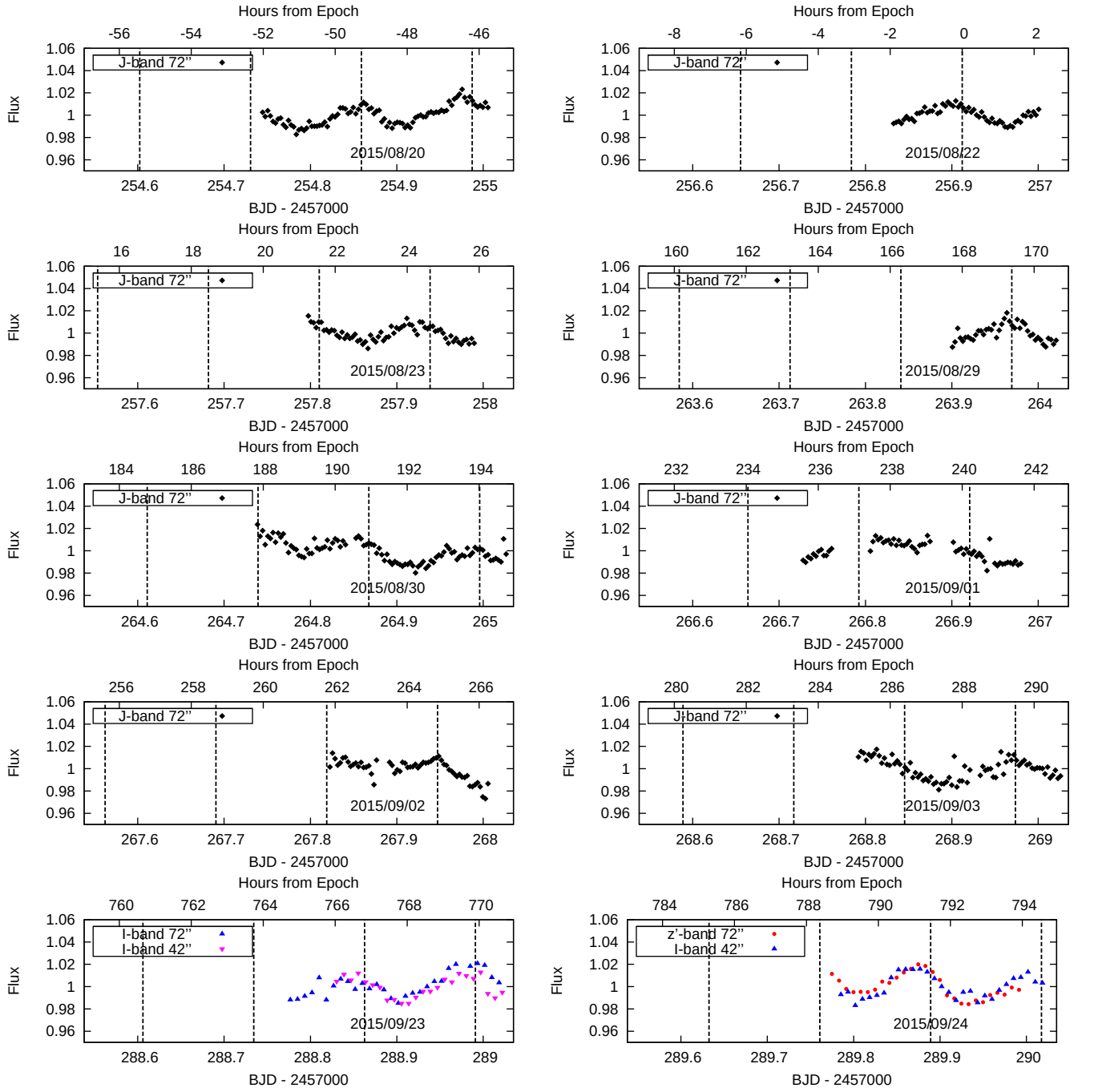

FIG. 1.— Photometry of 2MASS 0036+18 on the dates given in the lower-right of each panel (UT) with the Perkins 1.8-m (72”) and Hall 1.1-m (42”) telescopes at various wavelengths (from the I to the J-band) as indicated in the legend of each panel. The vertical dashed lines indicate cycles of the apparent ∼3.080 hour rotation period of 2MASS J0036+18, compared to the apparent flux maximum in our J-band photometry at a barycentric julian date (BJD) of: BJD-2457000 ∼256.91. For clarity we plot our photometry binned every 0.003 d (∼4.3 minutes) for panels featuring single wavelength photometry, and binned every 0.008 d (∼12 minutes) for panels featuring multiwavelength photometry.

is 3.080 ± 0.001 hours. We also present Lomb-Scargle periodograms of our individual photometric bands when there is more than one data-set in Figure 3. The periods of the peaks of the Lomb-Scargle periodograms for each individual wavelength of data are given in Table 2. The obvious secondary, tertiary, and other peaks in the periodograms of the various wavelengths of observations are day aliases of the main ∼3.080 hour period, due to the nightly observing cadence. We conservatively estimate the errors on the period using the full width half maximum of the envelope of periodogram values near the maximum period peak in the periodogram.

The most prominent periods in the Lomb-Scargle periodograms for our various wavelengths of observations seem to be consistent with one another, suggesting that if our different wavelengths of observations are penetrating to different depths in the atmosphere then we are not observing significant differential rotation at different depths in the atmosphere. Also, the most prominent period from all our data of ∼3.080 ± 0.001 hours, agrees

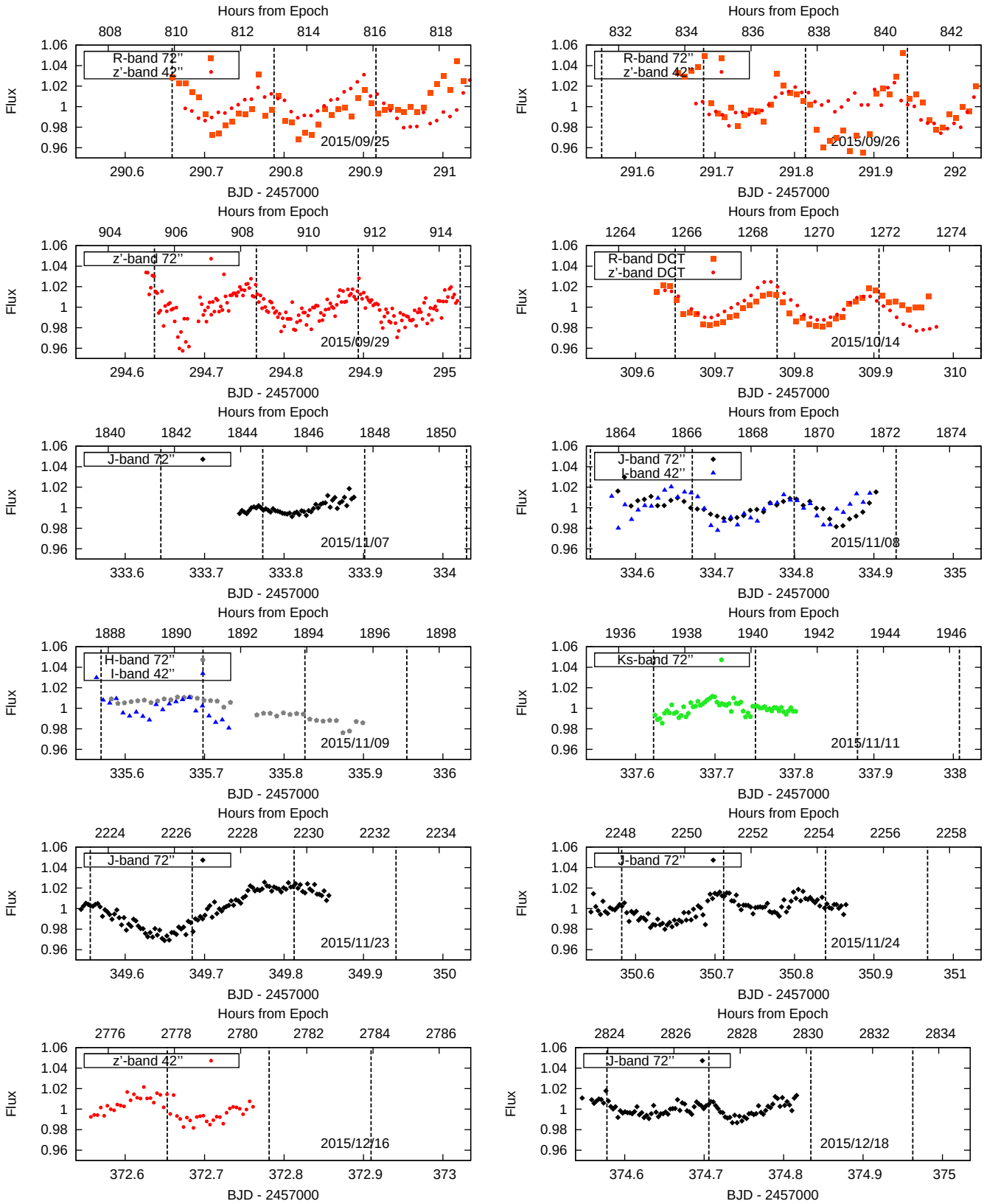

FIG. 2.— Photometry of 2MASS J0036+18 on the dates given in the lower-right of each panel (UT) with the Discovery Channel 4.3-m, Perkins 1.8-m (72") and Hall 1.1-m (42") telescopes at various wavelengths (from the R to the Ks-band) as indicated in the legend of each panel. The figure format is otherwise identical to Figure 1.

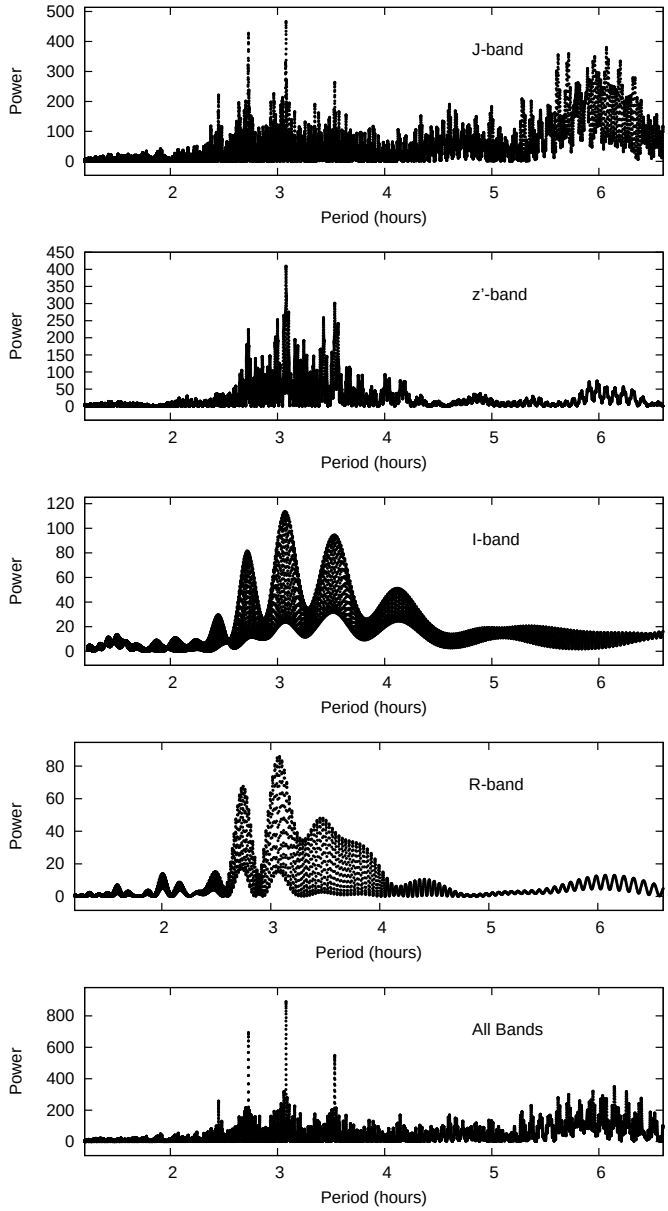

FIG. 3.— Lomb-Scargle Periodograms of our photometry of 2MASS 0036+18 in various bands as indicated in the panels, and with all our photometry (bottom). We present the peak periodogram values in Table 2, which are all approximately ∼3.08 hours.

TABLE 2
LOMB-SCARGLE PERIODOGRAM PERIODS OF VARIOUS BANDS OF OUR 2MASS 0036+18 PHOTOMETRY

Observing Band	Lomb-Scargle Peak Period P (hr)	# of light curves
R-band	3.081 ± 0.123	3
I-band	3.071 ± 0.125	5
z-band	3.079 ± 0.054	6
J-band	3.080 ± 0.005	13
All bands	3.080 ± 0.001	29

TABLE 3
SINUSOID FITS TO VARIOUS BANDS OF 2MASS 0036+18 PHOTOMETRY

Observing Band	Peak-to-Peak Amplitude A (%)	Phase (ϕ)	# of light curves
R-band	3.40 ± 0.11	0.884 ± 0.005	3
I-band	2.11 ± 0.09	0.879 ± 0.006	5
z-band	2.74 ± 0.08	0.878 ± 0.005	6
J-band	1.22 ± 0.04	0.913 ± 0.005	13
H-band	0.45 ± 0.05	0.869 ± 0.016	1
Ks-band	1.07 ± 0.08	0.628 ± 0.013	1
All bands	1.36 ± 0.03	0.896 ± 0.004	29
3.6 μm [a]	0.47 ± 0.05	n/a	1
4.5 μm [a]	0.19 ± 0.04	n/a	1

[a] The amplitudes at these wavelengths are included from 8 hours of 3.6 μm & 6 hours of 4.5 μm Spitzer/IRAC data (Metchev et al. 2015), respectively.

well with the 3.08 ± 0.05 hour radio period detected for this object by Hallinan et al. (2008). If the radio period results from the electron cyclotron maser instability from the polar regions of the ultra-cool dwarf (Hallinan et al. 2008), then the close similarity between the radio period and our optical/near-infrared period likely place a limit on differential rotation; if the radio period arises from deep within this ultra-cool dwarf, analogous to where the magnetosphere is believed to be generated from the core for Jupiter (Higgins et al. 1996), then the close correlation with our optical/near-infrared period shows the core magnetosphere rotates in phase with the photosphere. Our detected period is also in general agreement with the variety of other optical period detections for this object, including: ∼3.0 hours from I-band observations (Lane et al. 2007), & ∼3.0 ± 0.7 hours from I-band observations (Harding et al. 2013). Lastly our period is consistent with the 2.7 ± 0.3 hour period estimated from 14 hours of 3.6 & 4.5 μm infrared *Spitzer*/IRAC photometry of 2MASS 0036+18 (Metchev et al. 2015); these infrared wavelengths are likely to be probing lower pressure, and therefore higher altitude, regions of 2MASS 0036+18 than our optical/near-infrared observations, again placing a limit on differential rotation at different depths in the atmosphere.

4.2. *The Phase & Amplitude of 2MASS 0036+18's Multiwavelength Variability*

We phase our data in various bands to the apparent rotation period from all our data of ∼3.080 hours in Figure 4. Zero phase is defined at BJD-2457000 = 256.91 (corresponding to an apparent flux maximum in our J-band photometry). We fit sinusoids with this period to the photometry in various bands, allowing the peak-to-peak amplitude, A, and phase, ϕ, to vary for each individual band; these results are given in Table 3. ϕ is defined from 0 - 1 and $\phi = 0$ denotes the flux maximum of the sinusoid. In Table 3 we also include the peak-to-peak amplitudes returned recently for 2MASS 0036+18 at the 3.6 μm and 4.5 μm Spitzer/IRAC wavelengths (Metchev et al. 2015). With the caveat that our data and the Metchev et al. (2015) data were obtained many months apart, in general it is apparent that the amplitude of variability decreases as one moves to longer wavelengths.

There is also a statistically significant difference in ϕ

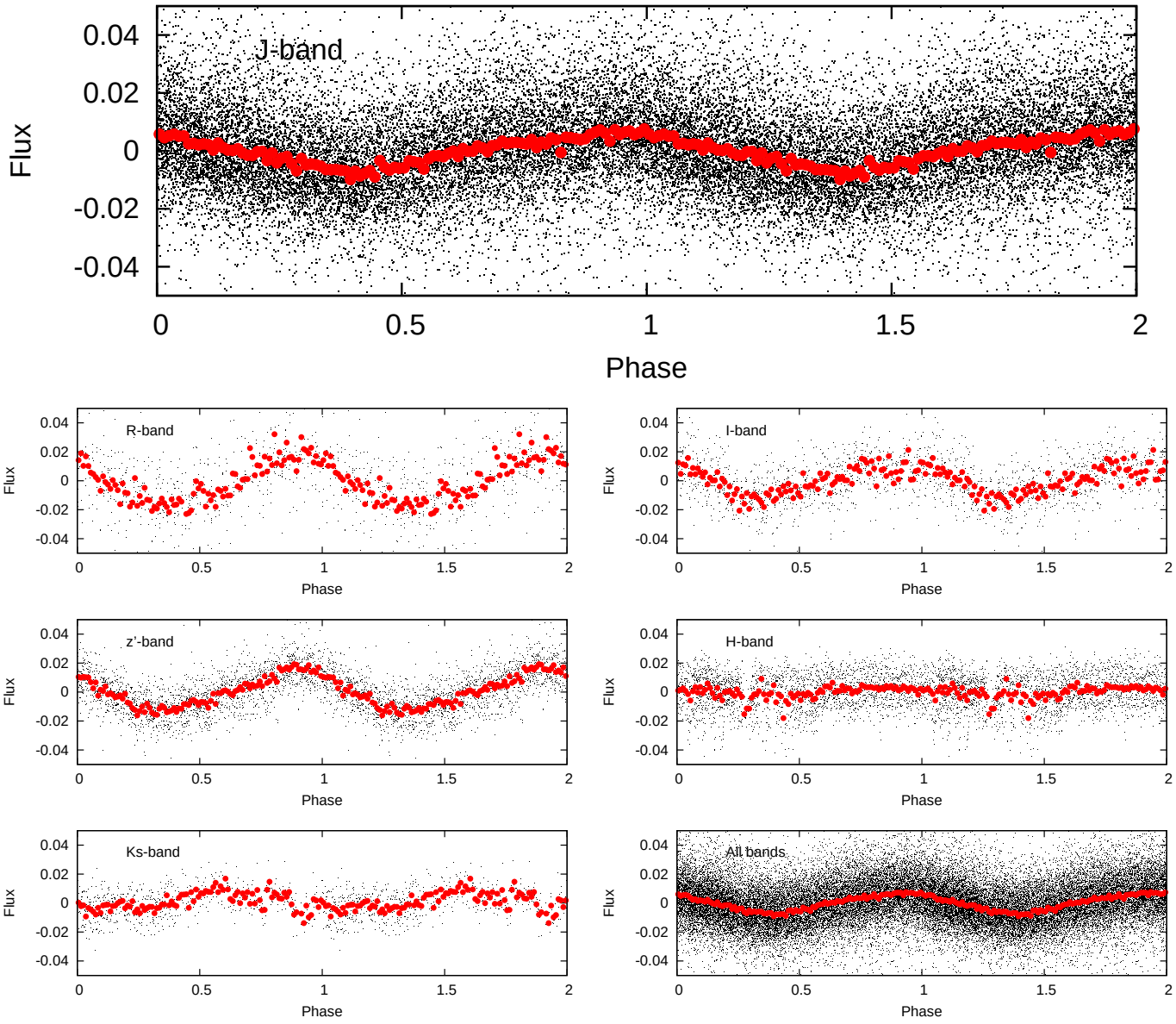

FIG. 4.— All our photometry of 2MASS 0036+18 (black points) in various-bands (as indicated in the panels) phased to the apparent rotation period of ∼3.080 hours. For clarity, the phase is plotted up to 2, and therefore two cycles are presented in each panel. Red circles denote the photometry binned every 0.01 in phase. Phase 0.0 is defined using the apparent flux maximum in our J-band photometry at BJD-2457000 ∼256.91. The number of light curves phased together to create each panel are given in Table 3.

values between the J-band photometry and some of the other photometric bands (z'-band for instance). As these light curves represent averages over up to ∼120 days of data, it is not clear whether these phase differences represent statistically significant phase offsets between various wavelengths of observations. Such apparent phase offsets may be caused by evolution in the longitude of starspot features from night-to-night and week to week, or a small mis-estimate of the true long-term period propagated over a great many rotation periods. An arguably superior way to determine whether there are statistically significant phase offsets between the near-sinusoidal variability at various wavelength of observations is to search for such phase offsets in multiwavelength data taken simultaneously.

Thus, we also fit our simultaneous multiwavelength light curves from a single night with sinusoidal fits. The associated amplitudes, A, and phases, ϕ, of the sinusoidal fits to each wavelength of photometry are shown in Figure 5, and Table 4. Most of the phase offsets between the various simultaneous wavelengths of photometry are not significant at the 3σ level. Our 2015 October 14th DCT light curve has an apparently significant phase offset; however, if we scale the reduced chi-squared of our sinusoidal fit to this light curve to 1 – to take into account the fact that the variability of 2MASS 0036+18 on this night may not be perfectly sinusoidal – then the phase offset is not significant at the 3σ level between the R-band and z'-band photometry.

We also investigate the evolution, or lack thereof, of the light curve of 2MASS 0036+18 with time. Specifically we investigate the change in amplitude of the variability of

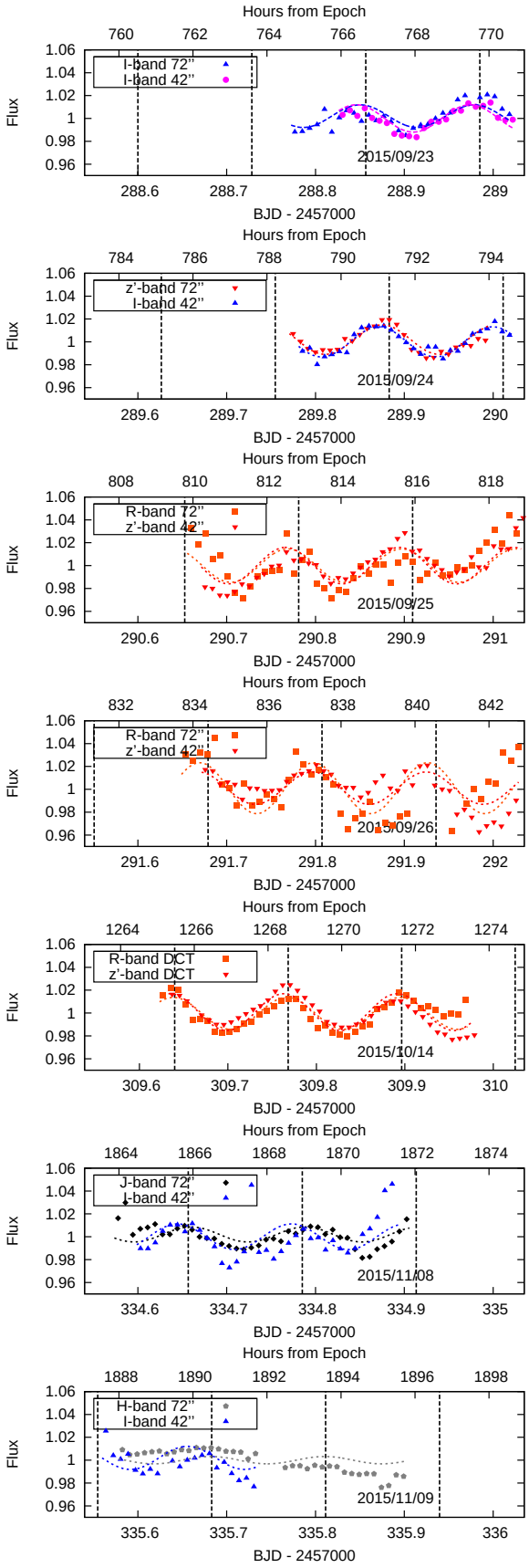

FIG. 5.— Sinusoid fits (dotted lines) to the simultaneous, multi-wavelength Perkins, Hall & DCT photometry of 2MASS 0036+18 in various bands. The colour of the dashed lines corresponds to the wavelength of observations as denoted by the colours of the data-points as indicated in the legend. The figure format is otherwise identical to Figures 1 & 2.

TABLE 4
SINUSOID FITS TO MULTIWAVELENGTH PHOTOMETRY OF 2MASS 0036+18

Date (UTC)	Telescope	Band	Peak-to-Peak Amplitude A (%)	Phase (ϕ)
2015/09/23	Perkins	I	1.98 ± 0.07	0.950 ± 0.005
2015/09/23	Hall	I	2.19 ± 0.15	0.929 ± 0.011
2015/09/24	Perkins	z'	2.51 ± 0.24	0.951 ± 0.013
2015/09/24	Hall	I	3.21 ± 0.17	0.921 ± 0.009
2015/09/25	Perkins	R	2.68 ± 0.16	0.922 ± 0.009
2015/09/25	Hall	z'	2.80 ± 0.26	0.918 ± 0.016
2015/09/26	Perkins	R	4.45 ± 0.10	0.926 ± 0.004
2015/09/26	Hall	z'	2.83 ± 0.09	0.914 ± 0.005
2015/10/14	DCT	R	2.78 ± 0.05	0.989 ± 0.003
2015/10/14	DCT	z'	3.22 ± 0.03	0.960 ± 0.002
2015/11/08	Perkins	J	1.22 ± 0.09	0.003 ± 0.010
2015/11/08	Hall	I	2.20 ± 0.30	0.951 ± 0.019
2015/11/09	Perkins	H	0.47 ± 0.06	0.989 ± 0.016
2015/11/09	Hall	I	2.08 ± 0.34	0.968 ± 0.028

2MASS 0036+18 from rotation period to rotation period, and night-to-night. For each complete rotation period of 2MASS 0036+18 we determine the peak-to-peak amplitude, ϵ, of the observed variability of that rotation period. To approximate ϵ we first exclude significant outliers (we cut out all data greater than 4 standard deviations from the mean); then we time-bin the data, by taking a running average of the photometry every 0.008 days (or ∼11.5 minutes). We then define ϵ as the difference between the maximum and minimum points of the time-binned data observed over each rotation period. We calculate ϵ for each complete rotation period that we have observed; a complete rotation period is defined when we have observed a full rotation period after the start of each night of observations (we also exclude ∼4 minutes at the start and end of each night of observations to avoid possibly, systematically biased photometry). We include rotation periods with small gaps of data missing due to clouds, or other telescope/instrument failures. We display a histogram of the peak-to-peak amplitude values, ϵ, for each complete rotation period for our J-band, z'-band & I-band photometry in Figure 6. Our J-band, z'-band & I-band histograms of our 2MASS 0036+18 photometry indicate that the variability we observe from 2MASS 0036+18 displays relatively constant amplitudes at these wavelengths; from rotation period to rotation period we appear to be observing modest amplitude evolution, but not nearly as significant as for our similar photometry of the L/T transition brown dwarf SIMP J013656.5+093347 (Croll et al. 2016). This lack of significant amplitude evolution appears to be consistent for the duration of our Fall 2015 observations of 2MASS 0036+18 (with the exception of our 2015 November 23 light curve; Section 4.4). The much more modest evolution in amplitude displayed by 2MASS 0036+18 compared to L/T transition brown dwarfs, suggests different variability properties on this L3.5 dwarf than brown dwarfs at the L/T transition.

We encourage continuing optical and near-infrared monitoring of this ultra-cool dwarf to determine how the variability amplitudes evolve in future observing sessions.

4.3. *Comparison to* v sin*i*

There have been a range of $v \sin i$ measurements for 2MASS 0036+18. We will henceforth utilize the $v \sin i$

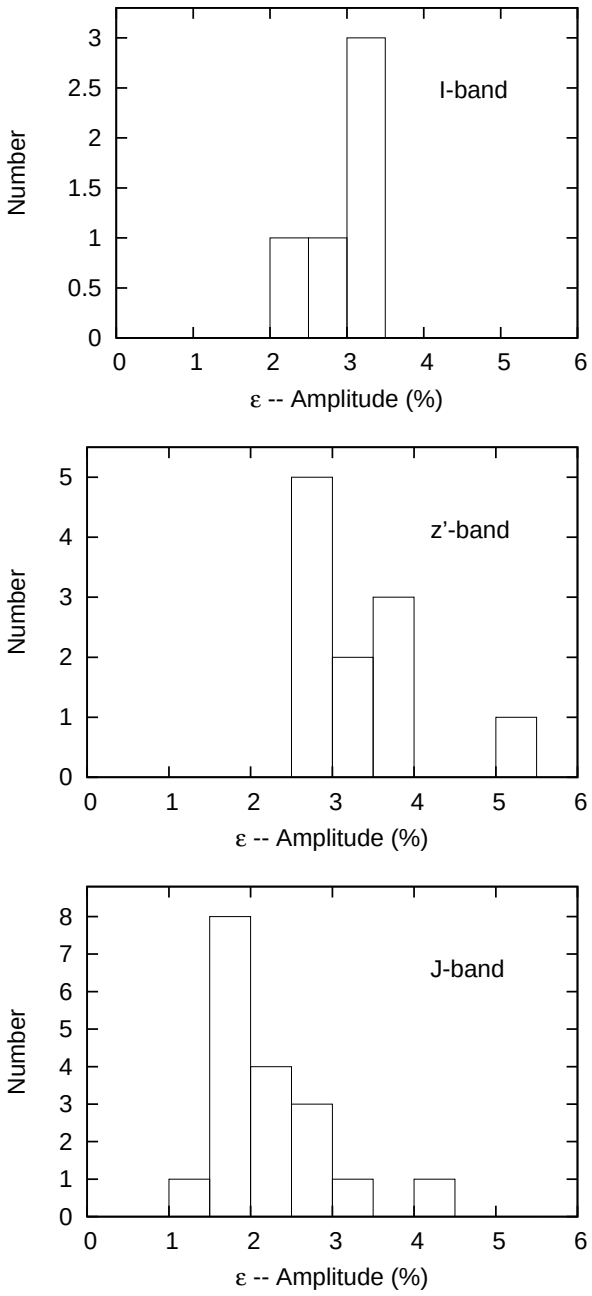

FIG. 6.— Histogram of the peak-to-peak amplitudes per complete rotation period, ϵ, of our photometry of 2MASS 0036+18 at various wavelengths, as indicated in the panels.

measurement quoted in Crossfield et al. (2014a), $v\sin i$ = 40.0 ± 2.0 km/s, a weighted mean of a number of different $v\sin i$ measurements (Jones et al. 2005; Zapatero Osorio et al. 2006; Reiners & Basri 2008) for this ultra-cool dwarf. Using the inferred radius of 2MASS 0036+18 of 0.09 ± 0.01 $R_{\odot}$ (Dahn et al. 2002), and our inferred rotation period of $P_{rot} = 3.080 \pm 0.001$ hr, this suggests a near edge-on inclination angle: $\sin i = 1.13 \pm 0.14$, or $i > 80^{o}$ (1σ error).

4.4. *Our 2015 November 23rd J-band light curve*

Our 2015 November 23rd J-band light curve of 2MASS 0036+18 displays a significantly longer period than our other light curves of this object. The Lomb-Scargle periodogram of this light curve indicates a period of 7.5± 0.9 hours, with a peak-to-peak amplitude of ∼4.6 %. A period approximately twice that of the rotation period we reach with the rest of our data (3.080 ± 0.001 hr) indicates the possibility that the actual rotation period is twice our inferred value, and that the variability we have been observing is due to two hot/cool spots on different sides of the ultra-cool dwarf. However, a ∼7.5 hour period would result in a $v\sin i$ estimate of ∼14.6 km/s (assuming an edge-on inclination angle), compared to the much larger measured value (40.0 ± 2.0 km/s; Crossfield et al. 2014a). We therefore do not find this possibility of a longer ∼7.5 hour rotation period for 2MASS 0036+18 compelling.

Another possibility is that the variability on that night is driven by another mechanism, unrelated to the rotation period of that ultra-cool dwarf. The significant growth of a spot or cloud clearing that is visible for a complete rotation period (e.g. a polar spot for edge-on inclination angles), or a multi-hour flare, could possibly explain our 2015 November 23rd J-band light curve. Significant growth (or decline) in the clouds that envelope 2MASS 0036+18, could also explain the observed variability, and mask the true rotation period of 2MASS 0036+18 (as suggested by Gelino et al. 2002) on that evening.

The last possibility is that systematic errors have affected the light curve on that evening. However, the weather was clear that evening, and we have ensured that the variability we observe on that evening is not due to a single reference star. Reference stars of similar brightness to 2MASS 0036+18, if analyzed utilizing the same techniques we apply to 2MASS 0036+18, do not display prominent variability on that evening, and therefore we have no strong evidence in favour that systematics affect our light curve. For this reason, we encourage further optical and near-infrared monitoring of this star to indicate whether variable light curves displaying periods longer than the rotation period we infer from our photometry (3.080 ± 0.001 hr) are observed for this ultra-cool dwarf.

5. A LIMIT ON OPTICAL/INFRARED FLARES

Our optical and near-infrared photometry of 2MASS 0036+18 also allows us to place a limit on the frequency of flares exhibited by this ultra-cool dwarf. 2MASS 0036+18 was observed to display a flaring event for ∼20 minutes from 3 hours of radio observations (Berger 2002); ∼18 hours of follow-up radio observations of 2MASS 0036+18 by Berger et al. (2005) did not detect flares, and placed a limit on radio flaring occurrences of <0.04 per hour. We do not see obvious signs of significant flaring activity in our 22 nights of optical and near-infrared photometry that consists of ∼180 hours of photometry. Inspection of the unbinned light curves suggests that we can conservatively rule-out[7] flares lasting twenty minutes or more that increase the optical or infrared flux by more than 10% in all our ∼180 hours of optical and near-infrared photometry, consisting of ∼150 hours of total, non-overlapping hours (excluding time when two telescopes are observing 2MASS 0036+18 at the same time). More stringent limits could likely be set

[7] Although please see the discussion in Section 4.4 about our 2015 November 23rd J-band light curve.

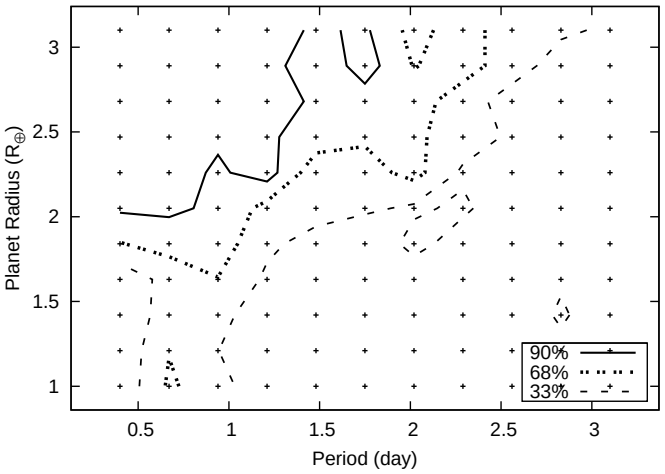

FIG. 7.— Percentage of inserted edge-on (i_p=90^o) transits (as indicated in the legend) that are recovered as a function of planet radius and orbital period using our multiwavelength ground-based photometry of 2MASS 0036+18. The small tick marks indicate the periods and radii at which signals from transiting planets were injected in the data.

using our photometric data-sets by applying a more detailed inspection of the light curves, including injection and recovery of putative flare events. We note that our limit on flares assumes that the persistent ∼3.080 hour variability we observe is not due to periodic flaring – a possibility suggested by Berger et al. (2005).

Our limit on optical and near-infrared flares is not stringent enough to suggest that the flare-rate of 2MASS 0036+18 is dissimilar to that of the L1 dwarf WISEP J190648.47+401106.8 (hereafter W1906+40); Gizis et al. (2013) presented 15 months of *Kepler* white light photometry of this ultra-cool dwarf, and suggested that the rate of energetic flares (>10^{31} erg) was approximately 1-2 per month (or ∼730 hours). The observed flares of W1906+40 (with energies > 10^{31} erg) increased the *Kepler* flux by up to four times the mean flux for durations of up to 1 hour. Simultaneous Gemini spectra suggested flare temperatures of 8000 ± 2000 K of W1906+40, meaning that the impact of flares of such temperatures would be diluted in our red optical and near-infrared photometry of 2MASS 0036+18, compared to the *Kepler* bandpass for Gizis et al. (2013) photometry of W1906+40. Nonetheless our much more stringent limit on flares, compared to the observed more frequent radio flares (Berger 2002; Berger et al. 2005), suggest that either the Berger (2002) observed radio flare occurs rarely, or that there is little correlation between radio flares and those observed in the optical & near-infrared (a conclusion similar to that reached from simultaneous optical & radio monitoring of two M8.5 dwarfs; Berger et al. 2008a,b).

6. SEARCHING FOR EARTH-SIZED PLANETS IN THE HABITABLE ZONE

Our multi-night, multiwavelength light curves also enable a search for transiting Earth-sized planets in the habitable zone of this brown dwarf. The inferred radius of 2MASS 0036+18 (0.09 ± 0.01 $R_\odot$; Dahn et al. 2002), means that even Earth-sized planets will display ∼1% transit depths. Using the inferred effective temperature of ∼1700 K (Cushing et al. 2008), planets with periods of a day or less to a few days will be sufficiently warm such that liquid water might be able to exist on these planet's surface (depending on the effects of tidal heating and the influence of various atmospheric compositions and albedos; Bolmont et al. 2011; Barnes & Heller 2013; Zsom et al. 2013).

Further motivation for searching for nearby companions in this system is provided by Berger et al. (2005) and Pineda et al. (2016); these authors suggest the possibility that the observed radio emission from 2MASS 0036+18 could result from tidal interactions with a close companion, analogous to Jupiter's interactions with its moon Io, or Saturn's interaction with its moon Enceladus. Berger et al. (2005) originally suggested the putative companion would have a ∼3 hour orbital period and tidal interactions would explain the periodicity in the radio observations of this system; Hallinan et al. (2008), however, explained the radio emissions as being due to the electron cyclotron maser instability. Nonetheless, Pineda et al. (2016) recently suggested that the observed Hα modulation of 2MASS 0036+18 could be induced by tidal interactions with a longer period planetary-mass companion.

Also, one might expect that if there is a planet in the system that it may very well lie along, or close to, the line of sight. This is because: (i) first of all, the comparison between the $v\sin i$ measurement and the rotation period for this ultra-cool dwarf suggests a near edge-on rotation angle, (ii) second, the conclusion of Albrecht et al. (2012) suggests that lower temperature stars seem to host spin-orbit aligned planets much more frequently than hotter stars, and this trend may continue into the sub-stellar regime.

To determine our ability to detect transiting, rocky exoplanets with our ground-based multiwavelength light curves of 2MASS 0036+18 we inject transits of simulated exoplanets into these light curves and test our ability to recover these planets. We use similar methodology to that presented in Croll et al. (2007a,b). We judge an inserted transit to be detected if the phase, ϕ_T, and period, P_T, returned by the transit search algorithm were sufficient close to the input parameters, P_{inp} & ϕ_{inp}. The detected period had to satisfy the following criterion: $|P_T/P_{inp} - 1| < 1\%$. If the transit routine returned an obvious harmonic of the orbital period (and the associated phase was incorrect), these periods were also judged to be detected; values up to four times the inserted period ($P_T \sim 4 \times P_{inp}$), or down to one-quarter the inserted period ($P_T \sim \frac{1}{4} \times P_{inp}$) were therefore accepted.

The results of these injection and recovery of transit simulations are presented in Figure 7. Our Monte Carlo simulations feature injected transits at 11 radii points and 11 period values, as indicated by the tick marks in Figure 7. For each radius, R_{inp}, and period, P_{inp}, value that transits were injected into the light curve for our Monte Carlo simulations, we repeat the injection and recovery for 21 random phase values at that radius and period value.

We note that much more stringent limits can likely be set from this photometry for our Monte Carlo tests by utilizing techniques to speficially detect single transit events. We have ruled out such single transit events by visual inspection for our photometry of 2MASS 0036+18,

but have not performed such inspection for our Monte Carlo data-sets.

We lastly note that we detect no compelling transiting planet signals in our ground-based photometry of this system. We therefore believe we can conservatively rule out edge-on transiting planets in this system with radii equal to or greater than those given in Figure 7 at the associated periods. As we have inspected our light curves for single transit events, we can likely set more stringent limits; we therefore believe that our photometry is sensitive to transiting planets as large or larger than super-Earths for most of the habitable zone around this ultra-cool dwarf.

7. THE PHYSICAL MECHANISM DRIVING VARIABILITY ON 2MASS 0036+18

Our 22 nights of photometry, including 7 nights of multiwavelength photometry, of 2MASS 0036+18 display a lack of obvious phase shifts between the variability observed simultaneously at different wavelengths, and variability amplitudes that generally decrease with increasing wavelength. Such behaviour is expected for starspot modulation, and is less consistent with variability driven by gaps in clouds, temperature variations, or aurorae, unless these other mechanisms only cause multiwavelength phase variations as small or smaller than what we have observed (Table 4). Starspot modulation causing the variability of 2MASS 0036+18 is also buttressed by the recent detection of Hα from 2MASS 0036+18 (Pineda et al. 2016). In Section 7.1 we present photometric starspot models that demonstrate that cool or hot spots can reproduce the profile of variability that we have generally observed for 2MASS 0036+18. In Section 7.2 we constrain the temperature of starspots on this ultra-cool dwarf, and demonstrate that spots $\sim$100 K cooler or hotter than the photosphere of 2MASS 0036+18 can explain the observed variability. In Section 7.3 we constrain the characteristics of clouds that are consistent with the variability that we observe on 2MASS 0036+18; gaps in clouds that reveal hotter layers underneath and span multiple pressure layers can explain the observed variability.

7.1. *Starspot model for 2MASS 0036+18*

We have attempted to reproduce the variability of 2MASS 0036+18 using a photometric starspot model. Our various 2MASS 0036+18 photometric light curves are fit using a Budding (1977) model utilizing the *StarSpotz* methodology (Croll et al. 2006; Croll 2006; Walker et al. 2007). Given that the combination of our inferred rotation period (3.080 $\pm$ 0.001 hr), and the $v$sin$i$ measurements for this ultra-cool dwarf suggest a near edge-on inclination angle (Section 4.3), the observed sinusoidal variability that persists for a large fraction of the rotation period is difficult to reproduce with a single spot, whether at low or high latitudes. Generically single spots at low latitudes for near edge-on inclination angles produce sharper decrements in flux that do not persist for a large fraction of the rotation period (e.g. the variability displayed in the 2003 MOST photometry of κ1 Ceti; Rucinski et al. 2004; Walker et al. 2007). Multiple spots appear to be required to reproduce the observed variability for 2MASS 0036+18 for near edge-on inclination angles. For spots near the equator for edge-on inclination angles, many spots will be required to reproduce the near sinusoidal variability; as few as two spots might reproduce the near sinusoidal variability if the spots are near the poles for near edge-on inclination angles. If we are viewing 2MASS 0036+18 at a low inclination angle, fewer star spots are likely required to reproduce the variability, although a near pole-on viewing geometry would be difficult to reconcile with the rotation period and $v$sin$i$ constraints for this object (see Section 4.3).

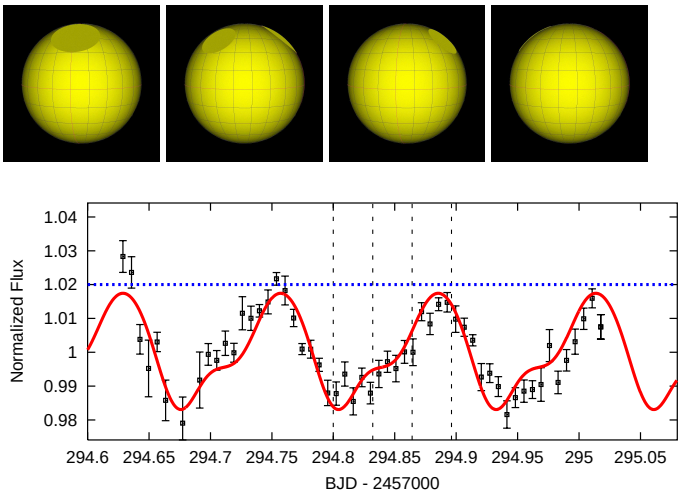

FIG. 8.— Top panels: possible spot model of 2MASS 0036+18 with cold spots (ΔT = -100 K) as seen from the line of sight at stellar rotation phases increasing (from left). The bottom panel displays our *StarSpotz* cold spot fit (the red solid curve) to our z'-band photometry (black points with error bars) on UT 2015/09/29. The blue horizontal dotted line displays the unspotted photosphere of the star. The vertical dotted black lines indicate the phases corresponding to the spot models in the top panels (increasing from left).

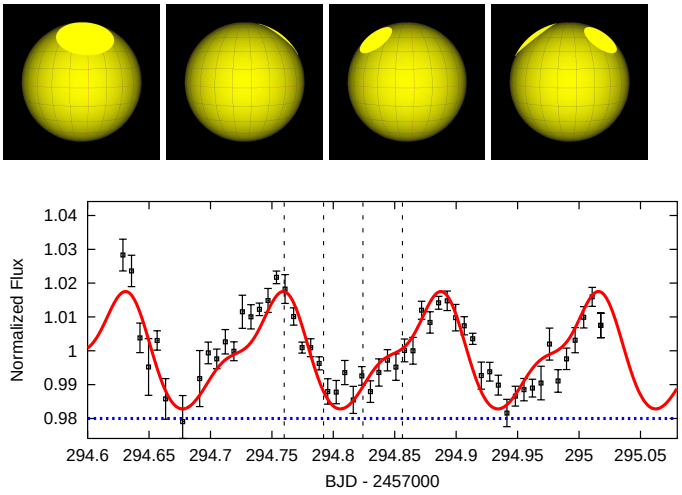

FIG. 9.— Top panels: possible spot model of 2MASS 0036+18 with hot spots (ΔT = +100 K) as seen from the line of sight at stellar rotation phases increasing (from left). The bottom panel displays our *StarSpotz* hot spot fit (the red solid curve) to our z'-band photometry (black points with error bars) on UT 2015/09/29. The figure is otherwise identical to Figure 8.

We present a possible two-spot model with cool spots for a near edge-on inclination angle for our z'-band light curve on UT 2015/09/29 in Figure 8. Also, spots hotter than the 2MASS 0036+18 photosphere are also able to reproduce the observed variability. We present a possible two-spot model with hot spots in Figure 9. These

models are not intended to display unique cold or hot spot solutions for the observed variability, as photometric starspot models are infamously non-unique (e.g. Croll 2006; Walker et al. 2007; Aigrain et al. 2015) - instead these models are simply intended to prove that cold and hot spot models with an edge-on inclination angle can reproduce the profile of variability generally displayed by 2MASS 0036+18.

7.2. *A limit on the Temperature of Starspots on 2MASS 0036+18*

If 2MASS 0036+18's variability is due to starspots then the multiwavelength amplitudes we observe allow us to place a limit on the temperature of these starspots compared to that of the photosphere. We first do this in Section 7.2.1 employing the approximation that 2MASS 0036+18 and its spots are blackbodies, to give a first-order approximation of the temperatures of spots on this L3.5 dwarf. Subsequently, in Section 7.2.2, we determine the temperature of starspots on this ultra-cool dwarf by comparing to one-dimensional cloud models.

For both the blackbody models and the one-dimensional cloud models, to facilitate this comparison we employ the method presented in Radigan et al. (2012). Equation 2 of Radigan et al. (2012) showed that the expected peak-to-peak variability amplitudes, A, driven by two regions with surface fluxes $\mathcal{F}_1$ and $\mathcal{F}_2$ rotating in and out of view can be expressed as:

$$A = \frac{(1-a-\Delta a)\mathcal{F}_1 + (a+\Delta a)\mathcal{F}_2 - (1-a)\mathcal{F}_1 - a\mathcal{F}_2}{0.5[(1-a-\Delta a)\mathcal{F}_1 + (a+\Delta a)\mathcal{F}_2 + (1-a)\mathcal{F}_1 + a\mathcal{F}_2]} \quad (1)$$

where a is the minimum filling factor of the $\mathcal{F}_2$ region on the ultra-cool dwarf, while Δa is the change in this filling factor. We assume that the atmosphere of 2MASS 0036+18 is dominated by the F_1 region of temperature T_{UCD} with small spots/clouds of different temperatures, T_{spot}, and associated surface fluxes F_2, rotating in and our of view. We assume $a = 0$ and therefore there is a time during each rotation period that no spots are in view along the line of sight.

For these comparisons, we assume that the variability of 2MASS 0036+18 is constant, and therefore we can utilize the amplitudes of variability observed at different wavelengths from different epochs (Table 3). This is likely a reasonable approximation given that we do not observe significant evolution in the variability amplitudes during our multiwavelength photometry from rotation period to rotation period (Figure 6). In Section 7.2.1 we also investigate whether different results are obtained if we allow the spot sizes to change with time and therefore must compare solely to the amplitudes from our simultaneous, multiwavelength photometry (Table 4). The conclusions we reach are qualitatively similar in both cases, and therefore henceforth make the assumption that the spot sizes are constant with time for most of the following analysis.

7.2.1. *Blackbody Models*

We first determine the temperature of starspots on 2MASS 0036+18 assuming that the ultra-cool dwarf and its starspots radiate like blackbodies. We use a $T_{UCD} = 1700\ K$ photosphere for 2MASS 0036+18 (Cushing et al. 2008 and see Section 7.2.2), and assume a single spot temperature. We employ Planck functions to calculate the flux for the ultra-cool dwarf, $\mathcal{F}_1$, and for the starspot, $\mathcal{F}_2$, with a temperature T_{spot}. As we assume $a = 0$ (and therefore there are times that no spots are visible), we compare the predicted variability amplitudes for different values of the change in filling factor, Δa, and the temperature of the spot, T_{spot}.

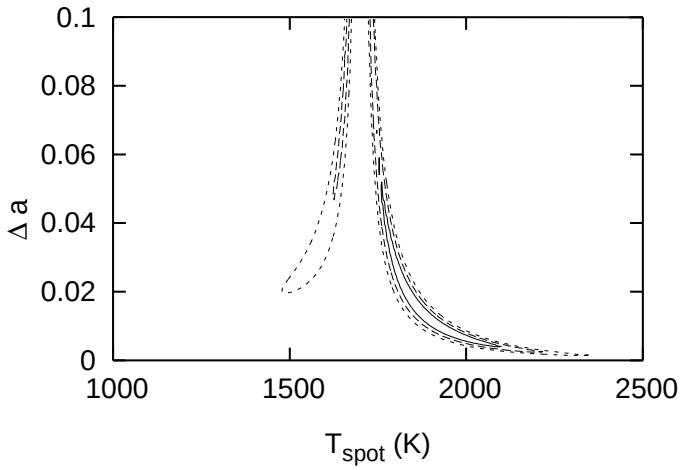

FIG. 10.— The change in filling factor, Δa (a proxy for spot size), and temperature of spots, T_{spot}, that are consistent with the amplitudes of sinusoidal variability observed at various wavelengths assuming the spots and 2MASS 0036+18 radiate like blackbodies. We assume constant spots and therefore compare to the amplitudes of multiwavelength variability observed at different epochs (Table 3). The solid-black, dashed and dotted lines are the 1σ, 2σ and 3σ credible regions, respectively. Starspots on 2MASS 0036+18 can be either slightly hotter or slighter cooler than the photosphere to be consistent with the amplitudes of variability that have been observed, if the spots and photosphere of this L3.5 dwarf radiate like blackbodies.

For the assumption of constant spots, and therefore constant multiwavelength amplitudes, we can compare to the multiwavelength amplitudes that have been observed previously at different epochs (Table 3). For blackbody emission, we present the best-fit spot temperatures in Figure 10. We scale the resulting reduced χ^2 to $\sim$1, to allow for reasonable-sized error bars on T_{spot}. The best-fit spot temperature can be slightly cooler than or slightly hotter than the photosphere of 2MASS 0036+18. The temperature is highly correlated with the assumed change in the filling factor, Δa, and therefore the size of the spots. For blackbody emission, if the spots are slightly cooler than 2MASS 0036+18 the allowed spot temperature ranges are approximately $T_{spot} = 1650 \pm 50\ K$, while if the spots are slightly hotter than 2MASS 0036+18 the allowed temperature ranges are approximately $T_{spot} = 1900 \pm 200\ K$.

We also compare our blackbody models to the measured amplitudes solely from our simultaneous, multiwavlength photometry (Table 4). We allow for different values of the change in filling factor (Δa) for each individual night of photometry, and attempt to determine the spot temperature, T_{spot}, that provides the best-fit (lowest χ^2) to our simultaneous, multiwavelength amplitudes. Utilizing a $T_{UCD} = 1700\ K$ photospheric temperature for 2MASS 0036+18, the best-fit spot temperature is approximately $T_{spot} < 1500\ K$ for the Table 4 simultaneous, multiwavelength amplitudes; this lower spot temperature is driven strongly by the 2015/10/14

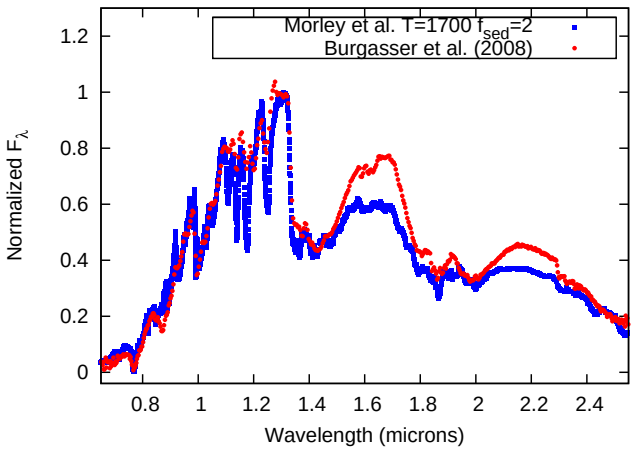

FIG. 11.— The Burgasser et al. (2008) spectra (red points) of 2MASS 0036+18 compared to the best-fit Morley et al. (in prep.) model spectra (blue points; utilizing $T_{UCD} = 1700\ K$, $log\ g \sim 5.5$, $f_{sed} = 2$).

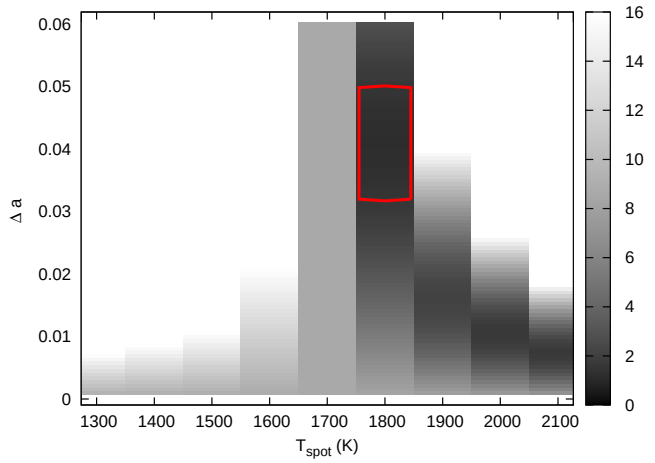

FIG. 12.— The change in filling factor, Δa (a proxy for spot size), and temperature of spots, T_{spot}, that are consistent with the amplitudes of sinusoidal variability observed at various wavelengths assuming the spots and 2MASS 0036+18 radiate according to the Morley et al. (in prep.) models. For 2MASS 0036+18 we utilize a Morley et al. (in prep.) model spectra with $T_{UCD} = 1700\ K$, $log\ g \sim 5.5$, $f_{sed} = 2$. We assume constant spots and therefore compare to the amplitudes of multiwavelength variability observed at different epochs (Table 3). The intensity bar at right denotes the reduced χ^2. The 1σ credible regions are enclosed in the red solid line. Spots $\sim$100 K hotter than our assumed $T_{UCD} = 1700\ K$ 2MASS 0036+18 photosphere provide the best-fits to our observed multiwavelength amplitudes.

DCT light curve, for which the measured R-band peak-to-peak amplitude (2.78 ± 0.05%) is less than the z'-band amplitude (3.22 ± 0.03%), and has the smallest associated error-bars of the amplitudes listed in Table 4. However, the 2015/10/14 DCT light curve ends at high airmass ($\sim$2.31); as the airmass increases that night the multiwavelength R-band and z'-band light curves diverge from their close agreement from earlier that evening. As we suspect this might be an airmass effect caused by the comparison of the redder target star to the bluer reference stars, we also repeat our analysis utilizing the 2015/10/14 DCT light curve with data later than BJD $\sim$309.9 excluded. The associated simultaneous, multiwavelength peak-to-peak amplitudes for our 2015/10/14 DCT light curve are then 3.36 ± 0.06% in R-band and 2.87 ± 0.03% z'-band. Utilizing this simultaneous, multiwavelength amplitude, and the others given in Table 4, the best-fit spot temperatures are $T_{spot} = 1600 \pm 100\ K$ for spots slightly cooler than 2MASS 0036+18, and $T_{spot} = 1750 \pm 50\ K$ for spots slightly hotter than 2MASS 0036+18. Therefore, using either our simultaneous, multiwavelength photometry (Table 4), or the assumption of constant spots (Table 3), the conclusions are similar in that the spots on 2MASS 0036+18 can be up to a few hundred degrees cooler or hotter than the 2MASS 0036+18 photosphere, if we assume the spot and ultracool dwarf radiate as blackbodies.

7.2.2. *Comparison to Models*

Although blackbody models are instructive, the spectrum of 2MASS 0036+18 deviates significantly from that of a blackbody (see Figure 11). If starspots exist on the surface of 2MASS 0036+18, then presumably the starspots on this ultra-cool dwarf also deviate significantly from blackbodies. Therefore, to perform a more realistic comparison, we next compare to one-dimensional cloud models of this L3.5 dwarf - these models will be presented in detail in Morley et al. (in prep.). These models are new, updated versions of the Saumon & Marley (2008) cloud models, which utilize the Ackerman & Marley (2001) cloud models. The models are coupled to one-dimensional pressure-temperature profiles of atmospheres in radiative-convective equilibrium. These models have varying effective temperatures, T, gravities, $log\ g$, and f_{sed} values. f_{sed} is a parameter that denotes the efficiency of sedimentation: high f_{sed} values (e.g. f_{sed}=5) result in vertically thinner clouds, while a low f_{sed} value (e.g. f_{sed}=1) results in thicker clouds.

To determine the characteristics of the unspotted photosphere of 2MASS 0036+18, we first compare the Morley et al. (in prep.) generated models to the Burgasser et al. (2008) spectra of 2MASS 0036+18 obtained with the SpeX prism instrument (Rayner et al. 2003) on the NASA Infrared Telescope Facility (IRTF). We test a limited grid of models from $T_{UCD} = 1500$ to 2100 K, $f_{sed} = 1$ - 2, and $log\ g \sim 4.5$ - 5.5. For these range of parameters the best-fit Morley et al. (in prep.) model is presented in Figure 11, and features the following parameters: $log\ g \sim 5.5$, $T_{eff} = 1700\ K$, and $f_{sed} = 2$. Our best-fit model underpredicts the H and K-band flux of 2MASS 0036+18, as these types of models often do for L-dwarfs (e.g. Figure 1 of Morley et al. 2012). Further comparisons of the 2MASS 0036+18 spectra to an expanded range of models that allow the metallicity, cloud patchiness, temperature variations, etc. to vary are warranted, but beyond the scope of this work.

As we are interested in the temperature of starspots that might be driving the variability of this ultra-cool dwarf, we first employ differences in temperature only, and not in cloud thickness, in our comparison of the Morley et al. (in prep.) models to Equation 1. Thus, we assume the $\mathcal{F}_1$ and $\mathcal{F}_2$ regions are identically cloudy ($f_{sed1} = f_{sed2} = 2$), although with different temperatures ($T_{UCD} \neq T_{spot}$).

We increment the T_{spot} values for the Morley et al. (in prep.) models in 100 K steps to calculate $\mathcal{F}_2$, and compare to the assumed best-fit photosphere of 2MASS

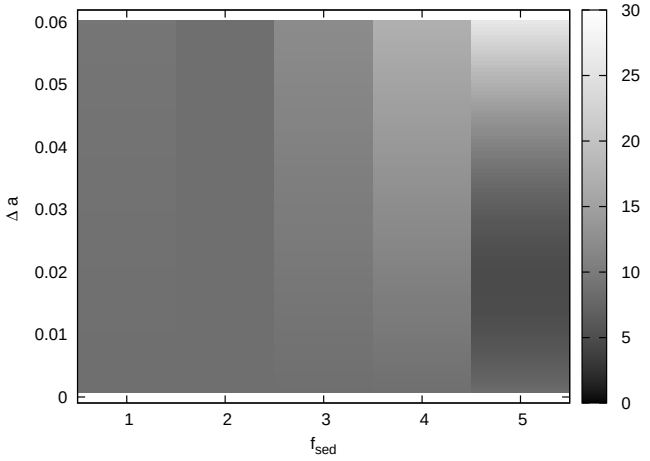

FIG. 13.— The change in filling factor, Δa (a proxy for spot size), and cloudiness parameter, f_{sed}, that are consistent with the amplitudes of sinusoidal variability observed at various wavelengths assuming the spots and 2MASS 0036+18 radiate according to the Morley et al. (in prep.) models. For 2MASS 0036+18 we utilize a Morley et al. (in prep.) model spectra with $T = 1700\ K$, $log\ g \sim 5.5$, $f_{sed} = 2$. The intensity bar at right denotes the reduced χ^2. We assume constant spots and therefore compare to the amplitudes of multiwavelength variability observed at different epochs (Table 3). None of these cloud models without temperature variations provide especially impressive fits to the observed amplitudes of variability.

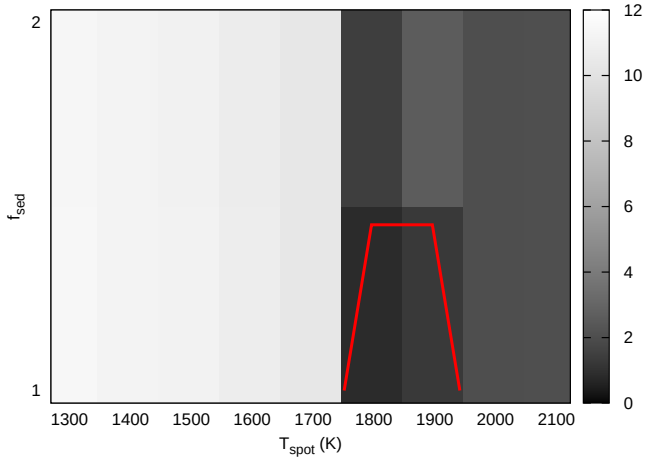

FIG. 14.— The change in spot temperature, T_{spot}, and cloudiness parameter, f_{sed}, that are consistent with the amplitudes of sinusoidal variability observed at various wavelengths assuming the spots and 2MASS 0036+18 radiate according to the Morley et al. (in prep.) models. For 2MASS 0036+18 we utilize a Morley et al. (in prep.) model spectra with $T = 1700\ K$, $log\ g \sim 5.5$, $f_{sed} = 2$. The intensity bar at right denotes the reduced χ^2. The 1σ credible region is enclosed in the red solid line (to the upper-right). We assume constant spots and therefore compare to the amplitudes of multiwavelength variability observed at different epochs (Table 3). Spotted regions slightly hotter than the 2MASS 0036+18 photosphere and with different cloud thicknesses can provide reasonable fits to the observed amplitudes of variability.

0036+18, $\mathcal{F}_1$ ($log\ g \sim 5.5$, $T_{UCD} = 1700\ K$, and $f_{sed} = 2$.). We integrate the Morley et al. (in prep.) models over the associated bandpasses of our observations (Table 3). We plot the best-fit models compared to our measured multiwavelength amplitudes (Table 3) for a range of Δa and T_{spot} values in Figure 12. We again scale the resulting reduced χ^2 to $\sim$1, to ensure reasonably-sized error bars on T_{spot}. The best-fit spot temperatures from the Morley et al. (in prep.) models are approximately $\sim$100 K hotter than the assumed $T_{UCD}\sim$1700 K 2MASS 0036+18 photosphere. As in Section 7.2.1 there is an obvious correlation between the size of spots, Δa, and the spot temperatures, T_{spot}, and small spots up to $\sim$300 K hotter than the assumed $T_{UCD}\sim$1700 K photosphere also provide reasonable fits to the multiwavelength variability.

As our fit to the 2MASS 0036+18 spectra suggests the presence of a considerable cloud layer enveloping 2MASS 0036+18, if starspots hotter than the photosphere of this ultra-cool dwarf are responsible for the observed variability there must exist some interplay between these two mechanisms. We explore the impact of clouds in Section 7.3, and discuss the interplay between these two mechanisms in Section 8.

7.3. *Clouds on 2MASS 0036+18*

We also explore whether cloud opacity variations could be driving the variability of 2MASS 0036+18. We note that if clouds, or aurorae, or another mechanism, are causing the variability on this ultra-cool dwarf then this mechanism must result in multiwavelength phase shifts smaller than we have observed in Table 4. If clouds exist on 2MASS 0036+18 and are causing the variability that we observe than the lack of significant multiwavelength phase shifts suggest that the cloud structures span multiple layers in the atmosphere of this L3.5 dwarf – specifically the cloud gaps must span the pressure layers probed by our simultaneous, multiwavelength photometry.

We first explore the possibility that varying cloud thicknesses on this L3.5 dwarf could be leading to the observed variability. We therefore employ a Morley et al. (in prep.) model where the spotted region has an identical temperature to that of 2MASS 0036+18, but different cloud thickness (i.e. $f_{sed1} \neq f_{sed2}$, $T_{UCD} = T_{spot}$). For 2MASS 0036+18 we again assume that the $\mathcal{F}_1$ region is composed of the values that provide the best-fit to the Burgasser et al. (2008) spectrum (Figure 11): $log\ g \sim 5.5$, $T_{eff} = 1700\ K$, and $f_{sed} = 2$. We increment the f_{sed} values by 1.0 and present the results in Figure 13. Of these varying f_{sed} models without temperature variations the best-fit to the observed amplitudes is provided by spots that are relatively cloud-free (f_{sed}=5). However, none of these cloud models without temperature variations provide impressive fits to the observed amplitudes; the varying temperature models (Section 7.2.2; Figure 12) provide considerably better fits to the observed amplitudes, than the models that allow the cloud thicknesses but not the temperatures to vary.

Therefore, if the 2MASS 0036+18 photosphere and spots follow the Morley et al. (in prep.) models, and if this ultra-cool dwarf displays constant amplitude variability, then clouds without temperature variations ($f_{sed1} \neq f_{sed2}$; $T_{UCD} = T_{spot}$) cannot be responsible for the variability we observe.

We next assume the spotted regions of 2MASS 0036+18 consist of different cloud thicknesses ($f_{sed1} \neq f_{sed2}$) and/or different temperatures ($T_{UCD} \neq T_{spot}$). We plot the best-fit comparisons to the data for a range of Morley et al. (in prep.) models with varying f_{sed2} and T_{spot} parameters in Figure 14. For this figure we only plot the optimal Δa parameter (lowest χ^2), for

the associated f_{sed2} and T_{spot} parameters. Spotted regions consisting of either different temperatures, or different cloud thicknesses and different temperatures provide reasonable fits to the observed amplitudes; the best-fit value is provided by a model with a slightly different cloud thickness (f_{sed}=1), and a different temperature ($T_{spot} = 1800\ K$) than our 2MASS 0036+18 photosphere. If the Morley et al. (in prep.) models provide reasonable approximations to the 2MASS 0036+18 photosphere and spotted regions, then spotted regions with different cloud thicknesses and temperatures ($f_{sed1} \neq f_{sed2}$ and/or $T_{UCD} \neq T_{spot}$) than this ultra-cool dwarf can explain the observed, multiwavelength amplitudes.

In general, according to our varying cloud thickness and varying spot temperature models, the best-fits to the observed amplitudes (Table 3) are provided by spots, or gaps in clouds, that are slightly hotter than the 2MASS 0036+18 photosphere. However, this conclusion depends on our assumption of constant spots and therefore that we can compare to our multiwavelength amplitudes observed at different epochs (Table 3); if the spots vary in size, a better comparison would solely be to our multiwavelength amplitudes observed simultaneously (Table 4). For the latter, simultaneous multiwavelength amplitudes, cooler spots than the 2MASS 0036+18 photosphere that radiate as blackbodies provide reasonable fits to the observed amplitudes (as discussed in Section 7.2.1). Therefore it seems prudent to conclude that spots up to a few hundred degrees cooler or hotter than the 2MASS 0036+18 photosphere can explain the observed multiwavelength variability of this ultra-cool dwarf.

8. CONCLUSION

Our long-term, multiwavelength, ground-based light curves of the L3.5 dwarf 2MASS 0036+18 allow us to address a number of unique science cases. First, our many nights of photometry allow us to demonstrate that the light curves of 2MASS 0036+18 do not significantly evolve from rotation period to rotation period, or night-to-night. This lack of evolution allows us to precisely determine the rotation period of this L3.5 dwarf to be 3.080 ± 0.001 hours. This rotation period is recovered from the R-band to the J-band, and is similar to the rotation period that has previously been recovered from radio (Hallinan et al. 2008) and infrared (Metchev et al. 2015) observations for this ultra-cool dwarf; therefore there is no strong evidence for differential rotation with latitude, or at different pressure layers as probed by shorter wavelength observations peering deeper into the atmosphere of this L3.5 dwarf.

These light curves also allow us to constrain the rate of flares exhibited by 2MASS 0036+18; this ultra-cool dwarf must display significantly fewer optical/near-infrared flares than radio flares (Berger 2002; Berger et al. 2005). Also, we are able to rule out transiting super-Earth, and even some Earth-sized planets in the habitable zone of this ultra-cool dwarf.

Our 7 nights of simultaneous, multiwavelength photometry do not display discernible phase shifts, and therefore suggest that the variability of 2MASS 0036+18 is driven by starspots, or another mechanism (clouds, aurorae, etc.) that results in similarly modest phase shifts. The amplitude of variability generally decreases with increasing wavelength, a result consistent with starspots slightly warmer or cooler than 2MASS 0036+18 being responsible for the observed variability, and with the Hα detection (Pineda et al. 2016) from this L3.5 dwarf. Our fit to the spectra of 2MASS 0036+18 suggests that considerable clouds envelope this ultra-cool dwarf. Clouds, or another mechanism, resulting in temperature differences could also be responsible for driving the observed variability of this ultra-cool dwarf, but this other mechanism would have to result in phase shifts as small or smaller than displayed in our multiwavelength photometry; therefore, if clouds are causing the variability of 2MASS 0036+18 then the gaps in clouds would likely have to span the multiple pressure layers probed by our observations and expose hotter layers of the atmosphere beneath the cloud layer. If a single mechanism is causing the variability of 2MASS 0036+18 then starspots or clouds that span multiple pressure layers are the leading explanations; however, other mechanism(s) that result in temperature differences, but a lack of significant multiwavelength phase shifts are also viable.

The lack of significant evolution of the 2MASS 0036+18 light curve from rotation period to rotation period, or night-to-night, is in stark contrast to what has been observed for L/T transition brown dwarfs (e.g. Artigau et al. 2009; Radigan et al. 2012; Gillon et al. 2013; Croll et al. 2016) and their variability that has generally been attributed to clouds. It is not clear if our detection of some, but not significant, evolution of the light curve of 2MASS 0036+18 favours an interpretation of clouds or spots driving the variability of this ultra-cool dwarf. Starspots on an active M-dwarf have been inferred to be quasi-stable for years (e.g. Davenport et al. 2015). Naively, one might expect cloud structures to evolve rapidly, but multiwavelength photometric monitoring of an L1 dwarf (Gizis et al. 2013, 2015) have indicated the possibility of a cloud feature that is stable on that ultra-cool dwarf for up to two years; in addition, Jupiter's Great Red Spot has likely been present since, at least, soon after the invention of the telescope (Hook 1665; Cassini 1666; Marcus 1993), suggesting that one cannot rule out a priori the presence of long-lived cloud structures on 2MASS 0036+18.

The most likely explanation for 2MASS 0036+18's variability is arguably a mixture of mechanisms. As our fit to the spectra of 2MASS 0036+18 suggests that significant clouds envelope this L3.5 dwarf, a mixture of clouds and starspots seems likely. The variability of 2MASS 0036+18 is likely driven predominantly by starspots, with some complex interplay between the hot/cool starspots and the clouds on this L3.5 dwarf that envelope this ultra-cool dwarf.

We encourage further long-term, multiwavelength monitoring of this intriguing L-dwarf, as well as other L and ultra-cool dwarfs, to determine the long-term variability amplitudes, phases, and evolution, or lack thereof, of these objects. With the recent detection that nearly all L-dwarfs are variable (Metchev et al. 2015), and that Hα detections are common for many early L-dwarfs (Schmidt 2015), such monitoring may indicate whether the observed characteristics of 2MASS 0036+18 are common for other early L-dwarfs.

We thank Dan Clemens for helpful discussions about

the Mimir non-linearity correction. We thank Francois-Rene Lachapelle, Etienne Artigau, & Sandie Bouchard for attempting to observe 2MASS 0036+18 simultaneously with our observations. We also thank Saul Rappaport for helpful discussions that improved this manuscript.

These results made use of Lowell Observatory's Discovery Channel Telescope. Lowell operates the DCT in partnership with Boston University, Northern Arizona University, the University of Maryland, and the University of Toledo. Partial support of the DCT was provided by Discovery Communications. LMI was built by Lowell Observatory using funds from the National Science Foundation (AST-1005313).

REFERENCES

Ackerman, A. S., & Marley, M. S. 2001, ApJ, 556, 872
Aigrain, S. et al. 2015, MNRAS, 450, 3211
Albrecht, S. et al. 2012, ApJ, 757, 18
Apai, D. et al. 2013, ApJ, 768, 121
Artigau, E. et al. 2009, ApJ, 701, 1534
Bailer-Jones, C.A.L. & Mundt, R. 2001, A&A, 367, 218
Barnes, J.R. & Collier Cameron, A. 2001, MNRAS, 326, 950
Barnes, J.R., James, D.J. & Collier Cameron, A. 2004, MNRAS, 352, 589
Barnes, R. & Heller, R. 2013, Astrobiology, 279, 291
Belu, A.R. et al. 2013, ApJ, 768, 125
Berger, E. 2002, ApJ, 572, 503
Berger, E. et al. 2005, ApJ, 627, 960
Berger, E. et al. 2008a, ApJ, 676, 1307
Berger, E. et al. 2008b, ApJ, 673, 1080
Biller, B.A. et al. 2013, ApJ, 778, L10
Bolmont, E. et al. 2011, A&A, 535, A94
Budding, E. 1977, Ap&SS, 48, 207
Buenzli, E. et al. 2012, ApJ, 760, L31
Buenzli, E. et al. 2014, ApJ, 782, 77
Buenzli, E. et al. 2015, ApJ, 798, 127
Burgasser, A. et al. 2008, ApJ, 681, 579
Cassini, G.D. 1666, Philosophical Transactions, 2, 615
Clarke, F.J. et al. 2002, MNRAS, 332, 361
Clarke, J.T. et al. 1980, ApJ, 241, L179
Clemens, D.P. et al. 2007, PASP, 119, 1385
Charbrier, G. et al. 2000, ApJ, 542, 464
Croll, B. 2006, PASP, 118, 1351
Croll, B. et al. 2006, ApJ, 648, 607
Croll, B. et al. 2007, ApJ, 658, 1328
Croll, B. et al. 2007b, ApJ, 671, 2129
Croll, B. et al. 2015, ApJ, 802, 28
Croll, B. et al. 2015b, ApJ, submitted, arXiv:astro-ph/1510.06434
Croll, B. et al. 2016, MNRAS, submitted
Crossfield, I.J.M. et al. 2014a, A&A, 566, A130
Crossfield, I.J.M. et al. 2014b, Nature, 505, 654
Cushing, M.C. et al. 2008, ApJ, 678, 1372
Dahn, C.C. et al. 2002, AJ, 124, 1170
Davenport, J.R.A. et al. 2015, ApJ, 806, 212
Dressing, C.D. & Charbonneau, D. 2015, ApJ, 807, 45
Fazio, G.G. et al. 2004, ApJS, 154, 10
Gelino, C.R. et al. 2002, ApJ, 577, 433
Gillon, M. et al. 2013, A&A, 555, L5
Gillon, M. et al. 2016, Nature, 553, 221
Gizis, J.E. et al. 2013, ApJ, 779, 172
Gizis, J.E. et al. 2015, ApJ, 813, 104
Harding, L.K. et al. 2013, ApJ, 779, 101
Hallinan, G. et al. 2008, ApJ, 684, 644
Hallinan, G. et al. 2015, Nature, 568, 568
Heinze, A.N. et al. 2013, ApJ, 767, 173
Higgins, C.A. et al. 1996, Geophysical Research Letters, 23, 2653
Hook, R. 1665, Philosophical Transactions, 1, 245
Howard, A.W. et al. 2012, ApJS, 201, 15
Irwin, J. et al. 2011, ApJ, 727, 56
Janes, K.A. et al. 2004, BAAS, 36, 672
Jones, H.R.A. et al. 2005, MNRAS, 358, 105
Lane, C. et al. 2007, ApJ, 668, L163
Littlefair, S.P. et al. 2008, MNRAS, 391, L88
Lomb, N. R. 1976, Ap&SS, 39, 447
Kao, M. et al. 2016, ApJ, 818, 24
Kirkpatrick, J.D. et al. 2000, AJ, 120, 447
Koen, C. 2013, MNRAS, 428, 2824
Maiti, M. et al. 2007, AJ, 133, 1633
Marcus, P.S. 1993, ARA&A, 31, 523
Massey, P. et al. 2013, AAS, 221, #345.02
Metchev, S.A. et al. 2015, ApJ, 799, 154
Mohanty, S. et al. 2002, ApJ, 571, 469
Morley, C.V. et al. 2012, ApJ, 756, 172
Morley, C.V. et al. in preparation
Morley, C.V. et al. 2014, ApJ, 789, L14
Muirhead, P.S. et al. 2012, ApJ, 747, 144
Pineda, J.S. et al. 2016, ApJ, 826, 73
Radigan, J. et al. 2012, ApJ, 750, 105
Radigan, J. et al. 2014, ApJ, 793, 75
Rayner, J.T. et al. 2003, ApJ, 115, 362
Reiners, A. & Basri, G. 2008, ApJ, 684, 1390
Robinson, T.D. & Marley, M.S. 2014, ApJ, 785, 158
Rockenfeller, B., Bailer-Jones, C.A.L. & Mundt, R. 2006, A&A, 448, 1111
Route, M. & Wolszczan, A. 2012, ApJ, 747, L22
Rucinski, S.M. et al. 2004, PASP, 116, 1093
Saumon, D. & Marley, M.S. 2008, ApJ, 689, 1327
Scargle, J.D. 1982, ApJ, 263, 835
Schmidt, S.J. 2015, AJ, 149, 158
Showman, A.P. & Kaspi, Y. 2013, ApJ, 776, 85
Snodgrass, C. & Carry, B. 2013, The Messenger, 152, 14
Vrba, F.J. et al. 2004, AJ, 127, 2948
Walker, G.A.H. et al. 2007, ApJ, 659, 1611
West, A.A. et al. 2004, AJ, 128, 426
Williams, P.K.G. & Berger, E. 2015, ApJ, 808, 189
Yang, H. et al. 2016, ApJ, accepted, arXiv:astro-ph/1605.02708
Zapatero Osorio, M.R. et al. 2006, ApJ, 647, 1405
Zsom, A. et al. 2013, ApJ, 778, 109